

ABSTRACT: The present study deals with a new type caisson, which has slitting half-circle wave chambers in front of the ordinary type. This caisson can reduce a peak value of the shock pressure with its two features i.e. half-circle and slit. The half-circle brings time delays of local shock pressures along its surface. The slit divides a peak of the shock wave force into two sub peaks with some time delay. These delays reduce total peak value of the shock wave. Compared with conventional caissons, about 60% reduction of the peak value of the shock pressure can be achieved. Two new theoretical models are developed to explain the reduction mechanisms and verified experimentally.

1. INTRODUCTION

Caisson type structures have been increasingly used for breakwater works following harbor expansions to deeper area. While they are constructed in shallow area, armor blocks have been used so as to reduce shock wave pressures. Since a cost of the block work increases with a water depth, demands for a new type caisson, which is capable of resisting to the shock pressure without blocks, have been increased. A present study deals with a new type caisson, which has half-circle wave chambers (Fig.1).

The conventional theoretical models for the shock wave pressure base roughly on the Karman model (1929) or Wagner model (1937). The Karman model is widely applied, since it explains the mechanism of the shock pressure very simply applying a momentum concept. However, this model is not capable of describing a detailed pressure distribution along an obstacle. On the other hand Wagner model bases on a potential theory and it is capable of calculating the pressure distribution. This theory models the obstacle with a flat plate. Due to the mathematical singularities, which appear at both ends of the plate, this model has been scarcely applied in the design of coastal structures regardless of some modifications made by Armand & Cointe (1986), Watanabe (1986).

The present study also bases on the potential theory and models a submerged part of the obstacle in water with an elliptic to avoid the singularity problem very simply. A function of the slit on the half-circle is also modeled theoretically applying the momentum concept.

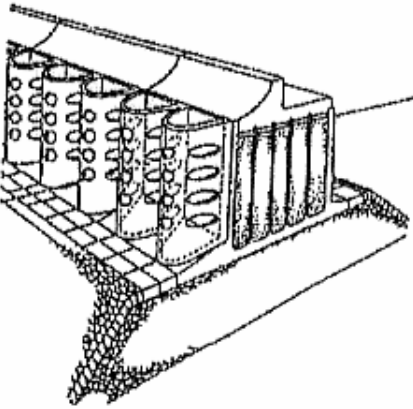


Figure 1 New type caisson

2. CONVENTIONAL MODELS

2.1 Karman model

Karman treated a dropping problem of a wedge into water. From the momentum conservation law, a force acts on the wedge given as

$$F = \frac{d(mV)}{dt} = m \frac{dV}{dt} + V \frac{dm}{dt}, \quad (1)$$

where m is a water mass which is accelerated by the wedge motion, V is a vertical wedge speed and t refers to time. If a mass of the wedge M is sufficiently large ($M \gg m$), dV/dt is very small and F is approximately proportional to dm/dt . Karman modeled the wedge with a thin plate. Its width is equal to a water line of the wedge. He approximated an added mass of the thin plate as

$$m = \frac{\rho \pi b^2}{2}, \quad (2)$$

where ρ is the water density and b is a half width of the plate. If t starts when the wedge first touch to the water surface, b is given as

$$b = 2Vt \tan \frac{\theta}{2}, \quad (3)$$

where θ is a top angle of the wedge. Substituting eqs.(2) and (3) into eq.(1), F is approximately derived as

$$F = 4\rho \pi V^3 t \tan \frac{\theta}{2}. \quad (4)$$

This model is applicable to the half-circle obstacle very simply. Figure 2 shows the half-circle. The half length of a water line on it is given as

$$b = \sqrt{R^2 - (R - Vt)^2}, \quad (5)$$

where R is a radius of the half-circle. Substituting eq.(5) into eq.(1), F is given as

$$F = \rho \pi R \{1 - t/(R/V)\} V^2. \quad (6)$$

When this model is used to evaluate wave pressure acts on the vertical wall, F becomes infinity, since $db/dt \propto (dm/db)^{1/2} \rightarrow \infty$.

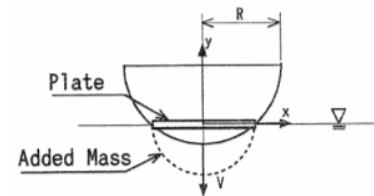


Figure 2 Karman model

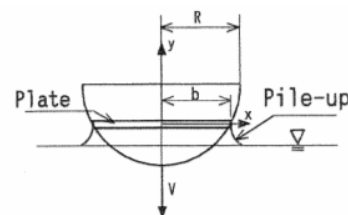


Figure 3 Wagner model

2.2 Wagner model

Wagner also approximated an obstacle in water with a flat plate. The plate and coordinates are shown in figure 3 when a half-circle is used as an obstacle. The complex velocity potential around a thin plate is given as

$$\omega = \phi + i\varphi = iV\sqrt{z^2 - b^2}, \quad (7)$$

where $i = \sqrt{-1}$, $z = x + iy$, ϕ and φ are the velocity potential and the stream function respectively. Special values for ϕ and φ are simply given as

$$|x| < b \text{ and } y = 0,$$

$$\phi = -V\sqrt{b^2 - x^2}, \quad \varphi = 0, \quad (8a)$$

$$|x| > b \text{ and } y = 0,$$

$$\phi = 0, \quad \varphi = V\sqrt{x^2 - b^2}. \quad (8b)$$

Substituting eqs.(8a,b) into the next pressure equation

$$\frac{p}{\rho} = -\frac{\partial\phi}{\partial t} - \frac{1}{2} \left\{ \left(\frac{\partial\phi}{\partial x} \right)^2 + \left(\frac{\partial\phi}{\partial y} \right)^2 \right\}, \quad (9)$$

pressure around the plate is obtained as

$$p = \frac{\rho V^2}{2} \left\{ \frac{2}{\sqrt{1 - (x'/b')^2}} \left(\frac{db'}{dt'} \right) - \frac{(x'/b')^2}{1 - (x'/b')^2} \right\}, \quad (10)$$

in which $x = x'/R$, $b' = b/R$ and $t' = t/(R/V)$.

Integrating p along the plate from $-b$ to b , wave force \int_w is obtained as

$$\int_w = \rho V^2 R \int_0^{b'} \left\{ \frac{2}{\sqrt{1 - (x'/b')^2}} \left(\frac{db'}{dt'} \right) - \frac{(x'/b')^2}{1 - (x'/b')^2} \right\} dx' \quad (11)$$

Wagner takes the piling-up of water surface into account. A half width of the water line b is derived in the present obstacle as follows.

From eq.(8a,b), water particle velocity v on the plate is derived as

$$v = \frac{\partial\phi}{\partial x} = \frac{V}{\sqrt{1 - (b/x)^2}} \quad (12)$$

The piling-up of water surface during time t to $t + dt$ is given as vdt . Its total amount from $t = 0$ to t is given as

$$y = \int_0^t \frac{V}{\sqrt{1 - (b/x)^2}} dt = \int_0^b \frac{V}{\sqrt{1 - (b/x)^2}} \left[\frac{dt}{db} \right] db. \quad (13)$$

A surface of the obstacle is approximated a series in his model.

$$y' = \beta_0 x' + \beta_1 x'^2 + \beta_2 x'^3 + \dots, \quad (14)$$

where $y' = y/R$ and $\beta_i, (i=1,2,\dots)$ is constants. Dividing eq.(13) with R and equating it with eq.(14), the next differential equation is obtained.

$$\frac{dt'}{db'} = \frac{2}{\pi} \beta_0 + \beta_1 b' + \frac{4}{\pi} \beta_2 (b')^2 + \frac{3}{2} \beta_3 (b')^3 + \dots \quad (15)$$

If the half-circle ($0 \leq x \leq b$) is approximated by

$$y' = \frac{x'^2}{2} + \frac{x'^4}{8} + \frac{3x'^{14}}{8}, \quad (16)$$

eq.(15) becomes to

$$\begin{aligned} \frac{dt'}{db'} &= -\frac{1}{2} b' + \frac{3}{16} b'^3 + \frac{9009}{8192} b'^{13} \\ &= \frac{4096 b' + 1536 b'^3 + 9009 b'^{13}}{8192}. \end{aligned} \quad (17)$$

Substituting eq.(17) into eq.(10), p is calculated. Figure 4 shows the distribution of p at shown time in the figure. A mathematical singularity ($p \rightarrow -\infty$) appears at $x' = b'$. Due to this singularity, application of this model has been very few in the design of coastal structures regardless of some modifications made by Armand & Cointe (1986) and Watanabe (1986).

3. ELLIPTIC MODEL

Figure 5 shows the caisson, half-circle and coordinates. x axis is taken on the water surface from the center line of the half-circle. y axis is taken upward from the water surface. The present theory uses an ellipse to model a submerged part of the half-circle. Semiaxes of the ellipse A and B are equal to a half width of the water line and a vertical length of the submerged part respectively. The piling-up of the water surface is not considered. The dropping speed of the half-circle is V . t starts when the half-circle first touches the water surface. A and B at time t are given as

$$A = \sqrt{R^2 - (R - Vt)^2}, \quad B = Vt. \quad (18)$$

The complex velocity potential of the steady flow around the ellipse is derived from a mapping of a flow around a cylinder. Figure 6 shows a circle and a ellipse. The circle K_t

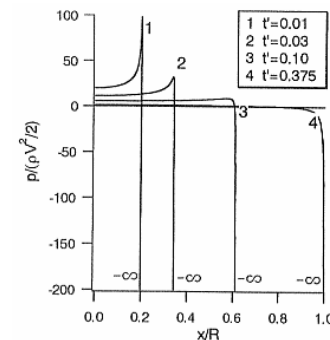


Figure 4 Pressure distribution (Wagner model)

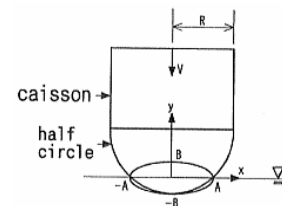


Figure 5 Half-circle and coordinates

with a radius R_ζ on the complex plane ζ , ($\zeta = \xi + i\eta$) is expressed as

$$\zeta = R_\zeta \exp(i\alpha), \quad (19)$$

where α is an anti-clockwise angle measured from ξ axis. This circle is mapped to an ellipse P_t on z plane applying the Joukowski transformation

$$\begin{aligned} (z = \zeta + a^2/\zeta) \text{ as} \\ z = x + iy = R_\zeta \exp(i\alpha) + a^2 \exp(-i\alpha)/R_\zeta, \\ x = (R_\zeta + a^2/R_\zeta) \cos \alpha, \\ y = (R_\zeta - a^2/R_\zeta) \sin \alpha. \end{aligned} \quad (20)$$

The equation of P_t is given by

$$\frac{x^2}{(R_\zeta + a^2/R_\zeta)^2} + \frac{y^2}{(R_\zeta - a^2/R_\zeta)^2} = 1. \quad (21)$$

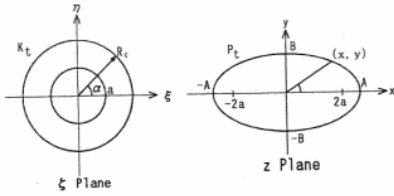


Figure 6 Mapped circle from the ellipse

Putting the semi-axes of eq.(21) equal to A and B in eq.(18) respectively, R_ζ and a in eqs.(19) and (20) are given as

$$R_\zeta = (A + B)/2, \quad a^2 = (A^2 - B^2)/4. \quad (22)$$

Applying these R_ζ and a in the equations from (19) to (21), eq.(19) becomes a mapped circle on ζ from the ellipse P_t on z by the Joukowski transformation. The complex velocity potential of the flow around K_t is given as

$$\omega_\zeta = iV \left\{ \exp(i\theta) + R_\zeta^2 \exp(-i\theta) / \zeta \right\}, \quad (23)$$

When V flows in η axis on ζ , $\theta = \pi/2$ and

$$\omega = iV(-\zeta + R_\zeta^2 / \zeta). \quad (24)$$

Applying the Joukowski transformation from z to ζ with

$$\zeta = \frac{z + \sqrt{z^2 - 4a^2}}{2}, \quad (x > 0), \quad (25)$$

the complex velocity potential around P_t is given as

$$\omega_\zeta = \frac{-iV}{2} \left\{ z + \sqrt{z^2 - 4a^2} - \frac{R_\zeta^2(z - \sqrt{z^2 - 4a^2})}{a^2} \right\}. \quad (26)$$

From eq.(9), p around P_t is determined by

$$\frac{p(z_p)}{\rho} = - \frac{\partial \phi}{\partial t} \Big|_{z=z_p} - \frac{u^2 + v^2}{2}, \quad (27)$$

where z_p indicates the points on P_t ($y < 0$). u and v are the water particle velocity in x and y directions respectively. The first term in eq.(27) is given as

$$\begin{aligned} \frac{\partial \phi}{\partial t} \Big|_{z=z_p} &= \text{Re} \left\{ \frac{\partial \omega_z}{\partial t} \right\} \\ &= \text{Re} \left\{ \frac{\partial \omega_z}{\partial z_p} \frac{dz_p}{dt} \right\} + \text{Re} \left\{ \frac{\partial \omega_z}{\partial a} \frac{da}{dt} \right\} + \text{Re} \left\{ \frac{\partial \omega_z}{\partial R_\zeta} \frac{dR_\zeta}{dt} \right\}, \end{aligned} \quad (28)$$

in which $\text{Re}\{ \}$ means a real part. From eq.(26), the first term in the second equation of eq.(28) is given as

$$\begin{aligned} \text{Re} \left\{ \frac{\partial \omega_z}{\partial z_p} \frac{dz_p}{dt} \right\} &= \text{Re} \left\{ - \frac{iV}{2} \left(1 + \frac{z_p}{\sqrt{z_p^2 - 4a^2}} \right) \frac{dz_p}{dt} \right. \\ &\quad \left. + \frac{iVR_\zeta^2}{2a^2} \left(1 + \frac{z_p}{\sqrt{z_p^2 - 4a^2}} \right) \frac{dz_p}{dt} \right\}, \end{aligned} \quad (29)$$

where

$$\begin{aligned} \frac{dz_p}{dt} &= \frac{u_{p\zeta} + iv_{p\zeta}}{1 - (a/R_\zeta)^2 (\cos 2\alpha + i \sin 2\alpha)}, \\ u_{p\zeta} &= (dR_\zeta / dt) \cos \alpha, \quad v_{p\zeta} = (dR_\zeta / dt) \sin \alpha. \end{aligned} \quad (30)$$

The second and third terms are also given as

$$\begin{aligned} \text{Re} \left\{ \frac{\partial \omega_z}{\partial a} \frac{da}{dt} \right\} &= \text{Re} \left\{ \frac{2iVa}{\sqrt{z_p^2 - 4a^2}} \frac{da}{dt} \right. \\ &\quad \left. + \frac{2iVR_\zeta^2}{a\sqrt{z_p^2 - 4a^2}} \frac{da}{dt} \right. \\ &\quad \left. - \frac{iVR_\zeta^2(z_p - \sqrt{z_p^2 - 4a^2})}{a^3} \frac{da}{dt} \right\}, \end{aligned} \quad (31)$$

$$\text{Re} \left\{ \frac{\partial \omega_z}{\partial R_\zeta} \frac{dR_\zeta}{dt} \right\} = \text{Re} \left\{ \frac{iVR_\zeta(z_p - \sqrt{z_p^2 - 4a^2})}{2a^2} \frac{dR_\zeta}{dt} \right\} \quad (32)$$

respectively where da/dt and dR_ζ/dt are derived from eqs.(18),(22) as

$$\frac{\partial a}{\partial t} = \frac{RV - 2V^2t}{4a}, \quad (33)$$

$$\frac{dR_\zeta}{dt} = \frac{V(R - Vt)}{2\sqrt{R^2 - (R - Vt)^2}} + \frac{V}{2}. \quad (34)$$

The second term in the second equation of eq.(27) is derived from

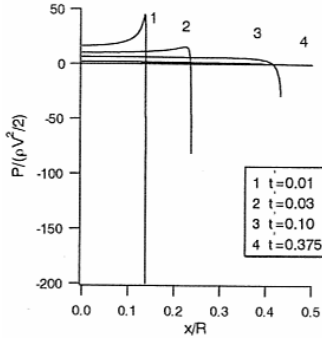


Figure 7 pressure distribution (Ellipse model)

$$u - iV = \frac{d\omega_z}{dz} = \frac{d\omega_z}{d\zeta} \frac{d\zeta}{dz} = \frac{d\omega_z}{d\zeta} \left(\frac{dz}{d\zeta} \right)^{-1} \quad (35)$$

$$= iV \left(-1 - \frac{R_\zeta^2}{\zeta^2} \right) \left(1 - \frac{a^2}{\zeta^2} \right)^{-1} = -iV \frac{1 + R_\zeta^2/\zeta^2}{1 - a^2/\zeta^2}.$$

Substituting eq.(19) in eq.(35), $u - iV$ is calculated as

$$u - iV = -iV \frac{\exp(-i\alpha)2 \cos \alpha}{1 - \frac{a^2}{R_\zeta^2} \exp(-2i\alpha)} \quad (36)$$

Applying the relation $u^2 + v^2 = (u - iV)(u + iV)$,

$$\frac{u^2 + v^2}{2} = \frac{1}{2} \left(-iV \frac{\exp(-i\alpha)2 \cos \alpha}{1 - \frac{a^2}{R_\zeta^2} \exp(-2i\alpha)} \right) \quad (37)$$

$$\times \left(iV \frac{\exp(i\alpha)2 \cos \alpha}{1 - \frac{a^2}{R_\zeta^2} \exp(2i\alpha)} \right)$$

$$= \frac{2V^2 \cos^2 \alpha}{1 - 2(a/R_\zeta)^2 \cos 2\alpha + (a/R_\zeta)^4}.$$

Substituting equations from (28) to (37) into eq.(27), pressure distribution around the ellipse can be calculated.

Figure 7 shows $p(z_p)$ at shown time t' in the figure. Individual lines in Figures 4 and 7 correspond with each other. Since piling-up of water surface is neglected in the present model, the values of t' in Figure 7 are selected so that the distances between the circle top and still water level in these figures are equal. $p(z_p)$ at side end of the ellipse show finite values regardless of t' .

4. VERIFICATION OF THE MODELS

4.1 Experiments

Figure 8 shows the experimental set up in a wave tank of 29m long, 0.5m wide and 0.75m deep. The model caisson with 3 half-circles (without slit) is placed on the steel mound. A radius of the half-circle is 8cm. $\pm 2.5\text{cm}$ interval of the central half-circle is replaced with a test section of the same radius. The test section is connected to a measuring instrument of wave force. The top figure in Figure 9 schematically shows a side view of the half-circle, coordinates, test section and breaking wave. β is an angle between a front surface of the wave and a vertical plane. The bottom figure shows a plan of the half-circle, a wave crest line, the model ellipse and coordinates. The water depth on the mound is 25cm in deep-water condition and 10cm in shallow-water condition. Preparatory experiments are made to find the wave conditions that bring the maximum shock wave force in the present wave tank (Fig.8). The wave conditions are listed in Table 1. The experiments are repeated 10 times with the same conditions.

4.2 Comparison of the model and the measurements

A horizontal component of the wave force acts on a unit height of the test section is given by the integration of $p(z_p)$ on the ellipse ($y < 0$) as

$$f_e(t) = \int_{z_p} p(z_p) \sin \gamma dz_p, \quad (38)$$

where γ is an angle between a tangent on z_p and y axis.

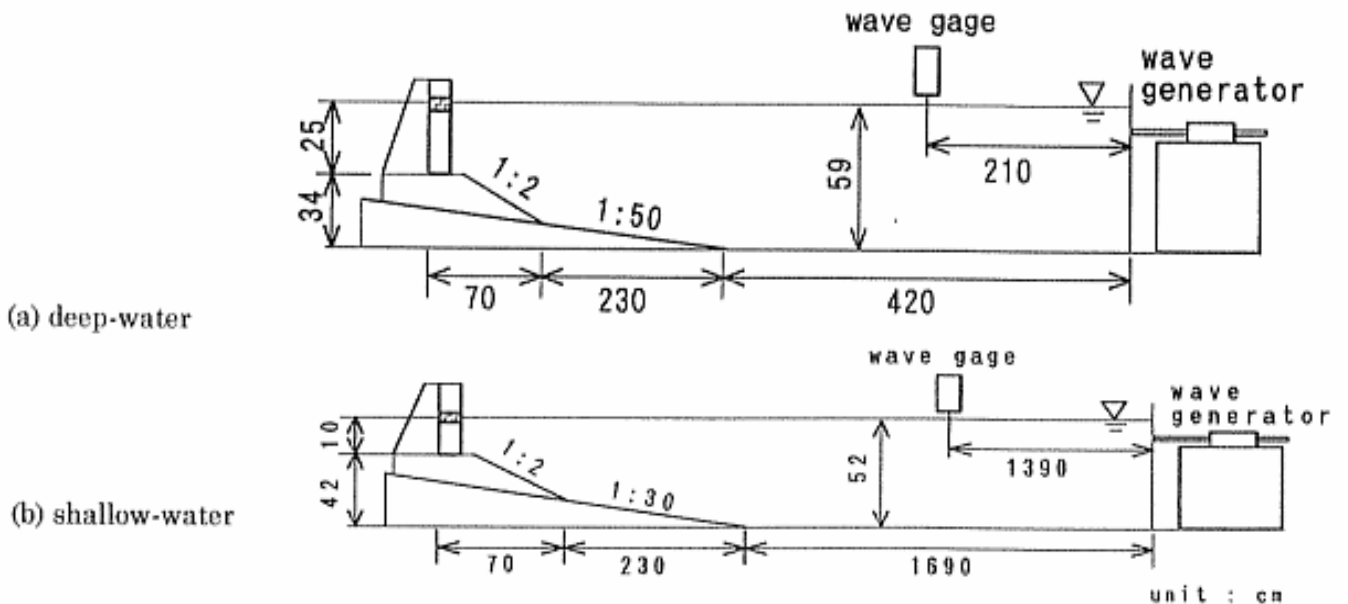


Figure 8 Experimental set up

The time when a wave starts to act on the circle at $z = z_u$ is given as $t = (z_u \tan \beta) / V$, in which V is the horizontal water particle velocity (Fig.9). The total wave force at this time is given as

$$F(t) = \int_0^{z_u} f_e \{t - t(z)\} dz, \quad (39)$$

where

$$f_e(t) = \begin{cases} 0 & : t \leq 0 \\ f_e(t) & : t > 0 \end{cases} \quad (40)$$

$F(t)$ is not calculated beyond the time $t = R/V$, since the wave front reaches to an end of the half-circle at $z = 0$ after this time. The peak value of the theoretical wave force appears before this time. In the experiments, it is also observed that a measured peak of the wave force appears

Table-1 Wave conditions

No.	Water depth	Wave height	Wave period
1	Deep water	27cm	1.3s
2	Shallow water	24cm	1.2s

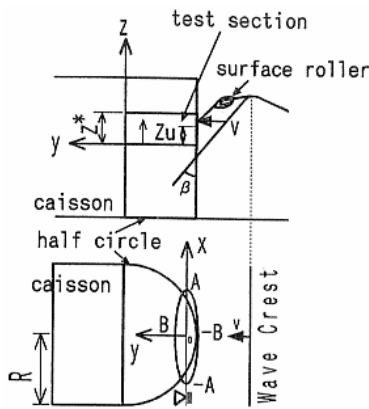
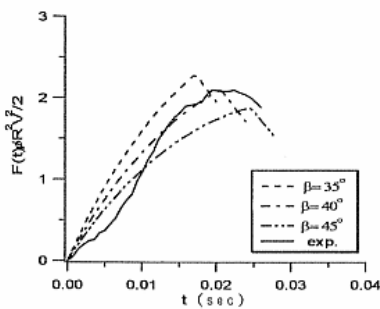
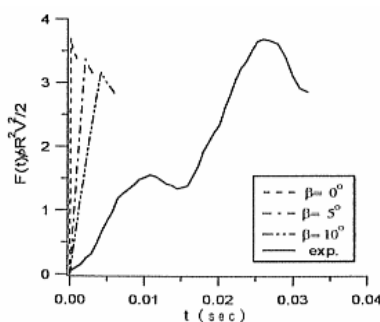


Figure 9 Side view (above) and plane (below)



(a) deep-water



(b) shallow-water

Figure 10 Profiles of the shock wave before the wave front arrives at an end of the half-circle at $z = 0$. Figure 10 shows examples of the measured (solid line) and calculated wave forces with three different β angles for (a) deep-water and (b) shallow-water conditions. The dynamic response of the measuring instrument, which appears on a record, is eliminated applying the method by Tanimoto et al. (1983). The measured values of β distribute around 40° in a deep-water condition and below 10° in a shallow-water condition. In the present theory, a peak on $F(t)$ appears at $t = 0$ when $\beta = 0^\circ$ in the shallow water condition. The discrepancy between the measured and the model profiles may be due to a response of the instruments (Tanimoto et al., 1983) Figure 11 shows the comparisons between the theoretical and the average values of the peak wave force in both conditions.

4.3 Size of the half circle

The time of the shock wave force from its start to the peak distributes between $1/100$ s – $4/100$ s in the experiments. If a radius of the half circle R is infinitely small compared with a wavelength, wave reaches to the caisson within this time. If R is very large, on the contrary, the half-circle works as a flat plate within the above time. The circle may not show its function to reduce the shock wave force in these cases. For effectiveness of the half-circle, it may be necessary that the submerged part be roughly $R/2$ within this time. This condition is expressed as

$$u_{\max} / 100 < R / 2 < 4u_{\max} / 100 \quad (41)$$

where u_{\max} is a horizontal water particle velocity. It is roughly 20% larger than the wave celerity when a wave breaks in a shallow water region.

5. FUNCTION OF THE SLIT

5.1 Experiments

The model tests are conducted to evaluate the function of the slit (holes) on the half-circle. The same wave conditions and the experimental setup are used (Fig.8). Figure 12 shows an appearance of the model caisson. The radius of the model half-circle is 8cm. Opening percentages of the slit on the half-circle are 15%, 30% and 45%. Shape of the slit (hole) is square and the sizes (height \times width) are

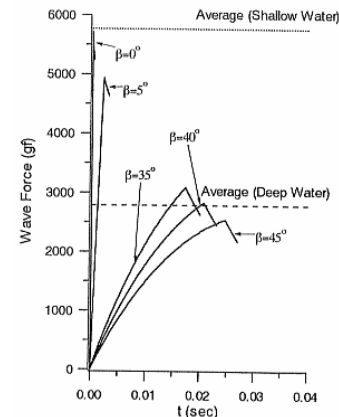


Figure 11 Theoretical shock wave profiles and averages of the measured data

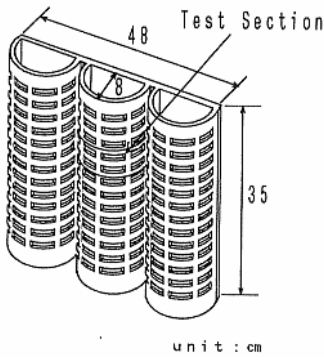


Figure 12 Model caisson

6mm × 36mm (15%), 12mm × 36mm (30%) and 15mm × 41mm (45%) respectively. Test sections with the same opening percentages are installed in the same position (Figs.8,9). Two extreme cases of 0% and 100% are also conducted. Those are a half-circle without slit (0%) and a caisson without the half circle (100%). A flat plate, which has a same projected area (5cm × 16cm) as that of the half-circle test section is installed on the vertical caisson surface (100%). Figure 13 shows the values of peak wave forces. Black circles (shallow-water condition) and black diamonds (deep-water condition) are the measured data and white marks are their mean at the same positions. The average data are listed in table-2. In the comparisons between the data at 0% and 100%, the present half-circle (0%) has a function to reduce the peak wave forces by roughly 20% in the deep-water condition and roughly 40% in the shallow-water condition respectively.

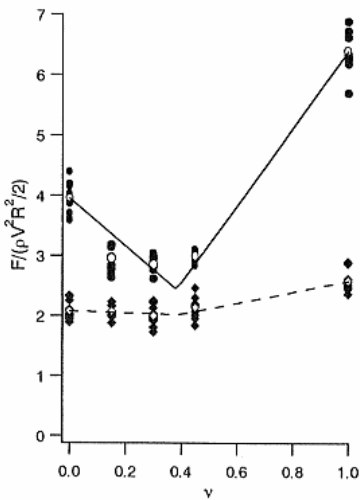


Figure 13 The peak wave force

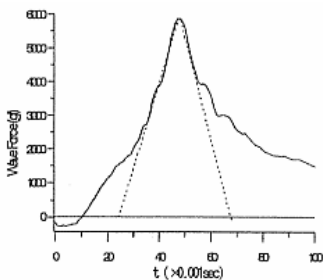


Figure 14 Modeling of the shock wave force

Table-2

	0%	15%	30%	45%	100%
Shallow Water	5770	4307	4165	4368	9339
Deep Water	2789	2771	2679	2866	3470

unit : gf

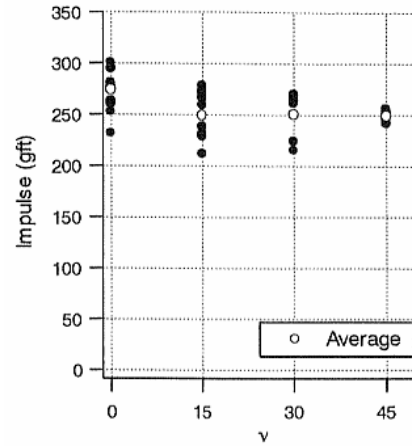


Figure 15 Total impulse

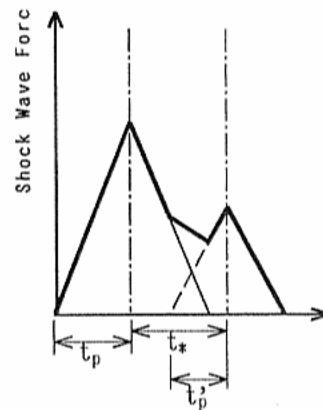


Figure 16 Modeling of a shock wave force with triangles (shallow-water)

The slit shows additional function of wave force reductions. When an opening percentage is 30%, the peak value is roughly 60% smaller compared with that of 100% in a shallow-water condition.

5.2 Modeling of a function of the slit.

A shock wave force is commonly modeled by a triangle. Figure 14 shows an example of the measured wave force (solid line) in a shallow-water condition and model triangle (dotted line). Integration of the area under the triangle may give an impulse brought about by the breaking wave (Fig.15). Average values (white circles) are almost constant for all cases. This may show the conservation of momentum.

a) Shallow-water condition

When a breaking wave hits the half-circle, first triangle appears. A part of the water spouts into the wave chamber through the slit. After a very short time, the second triangle appears when the water hit the caisson surface. Figure 16 schematically shows the shock wave force (two isosceles

triangles). t_p and t_p' are the half of their duration. t^* is an interval between the peaks. Measured wave force is modeled by the summing up of these triangles. If $t_p, t_p' < t^*$, two peaks appear on the sum and their heights are equal to their peak values.

In the shallow water condition, a water level in a wave chamber is very low just before the wave hit on the half-circle, waterspout through the slit may meet no water in the wave chamber and hit the caisson surface directly. t^* may be larger than t_p and t_p' in this case.

When a breaking wave hit the half-circle with a speed u_{\max} and its duration time is $2t_p$, a horizontal momentum brought about by the wave on the half-circle test section is

$$2\rho u_{\max}^2 R t_p z^*, \quad (a)$$

where ρ is the fluid density, z^* is a height of the test section. The momentum transferred through the slit into the wave chamber during $2t_p$ is given as

$$2\rho u_{\max}^2 R v t_p z^*, \quad (b)$$

where v is an opening percentage of the slit. Since t_p is very short, the water particle velocity may not change during the hit and spout. The difference between (a) and (b)

$$2\rho u_{\max}^2 R(1-v)t_p z^*, \quad (c)$$

may be equal to an impulse of the shock wave force acts on the half-circle. It is approximated with isosceles triangle in the present model. Solid thin line shows the wave force acts on the half-circle and broken line shows the wave force act on the caisson. The area of two triangles (impulses) are $t_p f_1$ and $t_p' f_2$ respectively in with f_1 and f_2 are their peak values respectively. Putting $t_p f_1$ and $t_p' f_2$ are equal to (c) and (b) respectively, f_1 and f_2 are calculated as

$$\begin{aligned} f_1 &= 2\rho u_{\max}^2 R(1-v)\lambda z^* \\ f_2 &= 2\rho u_{\max}^2 R v z^* \end{aligned} \quad (42)$$

where $\lambda = t_p' / t_p$. Since λ is also derived by a division of f_1 at $v = 0$ with f_2 at $v = 1$, $\lambda (< 1.0)$ gives a peak wave force reduction factor of the half-circle without the slit compared with that on a vertical wall. This reduction may be brought about by the time delays of local shock wave pressures along the half-circle.

The measures peak wave force is expressed as

$$F = \max(f_1, f_2). \quad (43)$$

Calculated value of λ is 0.61 when the average values in the table-2 are used. Solid line in Figure 13 shows eq.(43). Since it was very difficult to measure u_{\max} accurately, the line is drawn so that it passes on the average values of F at $v = 0$ and 1. The minimum value appears when $v = 0.38$. The peak wave force acts on the half-circle with slit reduces a peak value of the shock wave force by roughly 60% compared with a vertical wall at this opening percentage in the shallow-water condition.

b) Deep-water condition

Since a difference in water levels inside and outside the

wave chamber is not large in a deep-water condition, waterspout hit the water inside the wave chamber first. The momentum is transferred through the water in the wave chamber. The time for the momentum transfer from the half-circle to the caisson surface may be shorter than in the shallow-water condition. Figure 17 also shows the shock

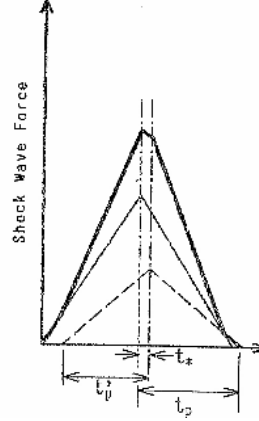


Figure 17 Modeling of a shock wave pressure with triangles (deep-water)

pressures in a deep-water condition schematically (two isosceles triangle). A surface roller of the breaking wave induces the shock wave force in this condition. The roller entrains some air in it. Since the same test section is used in the measurements, (a), (b), (c) and eq.(42) are modified as

$$2\rho u_{\max}^2 R t_p z^* \mu \quad (a')$$

$$2\rho u_{\max}^2 R v t_p z^* \mu \quad (b')$$

$$2\rho u_{\max}^2 R(1-v)t_p z^* \mu \quad (c')$$

$$\begin{aligned} f_1 &= 2\rho u_{\max}^2 R(1-v)\lambda z^* \mu \\ f_2 &= 2\rho u_{\max}^2 R v z^* \mu \end{aligned} \quad (44)$$

where μ is the ratio between a volume of air and total volume of air and water in the surface roller.

Putting

$$c = 2\rho u_{\max}^2 R v z^* \mu \lambda, \quad (45)$$

f_1 and f_2 are expressed as $c(1-v)$ and $c v / \lambda$ respectively. Dividing average value of f_1 at $v = 0$ with that of f_2 at $v = 1$ listed in the table-2, λ is calculated as 0.81. Since the second isosceles triangle overlap over the first one around their peaks, the maximum value of a sum is given as,

$$\begin{aligned} F &= \max \left\{ c(1-v) + c \frac{t_p' - t^*}{t_p} \frac{v}{\lambda}, \quad c \frac{v}{\lambda} + c \frac{t_p - t^*}{t_p} (1-v) \right\} \\ &= \max \left\{ c(1-v) + c \frac{\lambda t_p - t^*}{\lambda t_p} \frac{v}{\lambda}, \quad c \frac{v}{\lambda} + c \frac{t_p - t^*}{t_p} (1-v) \right\} \end{aligned} \quad (46)$$

Broken line in Figure 13 shows a comparison between the theoretical and measured peak values of F when $t^*/t_p = 0.2$. Since the measurements of the values of t^*/t_p , μ and u_{\max} are very difficult, the curves are drawn so that they pass

the average data at $v=0$ and 1. The smallest value appears at $v=0.40$ regardless of t^*/t_p . The peak wave force acts on the half-circle with slit is smaller than that on the vertical wall by roughly 40% in a deep-water condition.

This study deals with a new type caisson, which has slitting half-circle wave chambers in front of the ordinary caisson. This caisson has a function of shock wave force reduction. This function comes from its features i.e. half-circle and slit.

A new theoretical 'Elliptic' model, which bases on the potential theory, is derived to evaluate the shock wave pressure on the half-circle. This model is free from the singularity problem. This model shows good agreements with the measurements, although standing up time of the shock wave force is shorter than the measurements in a shallow water condition. This may be due to the measuring instrument. Also a new theoretical model, which bases on the momentum principle, is derived to evaluate the function of the slit. The model shows that an opening percentage of roughly 40% brings the largest reduction efficiency. The peak values reduce by roughly 40% in a deep-water condition and by roughly 60% in shallow water condition with the present caisson compared with the ordinary caisson.

REFERENCES

- Armand, J.L. & Cointe, R (1986): Hydrodynamic impact analysis of cylinder, Proc. 5-th Intl. OMAE Sympo, Vol.1.
- Tanimoto et al. (1983): Estimation method of exciting force from a response in a linear damped vibration system. Tech. Note of PHRI, No.474, 24p.
- Von Karman, Th (1929): The impact on seaplane floats during landing, NACA, TN321.
- Wanger, H. (1932): Uber stoss und gleitvorgange ander oberflache von flussigkeiten, Zeitschrift fur angewandte mathematik und mechanik, Band 12, Heft 4, pp.193-215.
- Watanabe, I. (1986): Analytical expression of hydrodynamic impact pressure by matched asymptotic expansion technique, Trans. West-Japan Soc. Nav. Archit., Vol. 71.